

## DIRECT NUMERICAL SIMULATION OF COMPLEX MULTI-FLUID FLOWS USING A COMBINED IMMERSSED BOUNDARY (IB) AND VOLUME OF FLUID (VOF) APPROACH

Niels G. DEEN, Martin VAN SINT ANNALAND and J.A.M. KUIPERS

University of Twente, Fac. of Science and Technology, PO Box 217, 7500 AE Enschede, THE NETHERLANDS

### ABSTRACT

In this paper a simulation model is presented for the Direct Numerical Simulation (DNS) of complex multi-fluid flows in which simultaneously (moving) deformable (drops or bubbles) and non-deformable (moving) elements (particles) are present, possibly with the additional presence of free surfaces. Our model combines the VOF model developed by van Sint Annaland et al. (2005) and the Immersed Boundary (IB) model The Volume of Fluid (VOF) part features i) an interface reconstruction technique based on piecewise linear interface representation ii) a three-dimensional version of the CSF model of Brackbill et al. (1992). The Immersed Boundary (IB) part incorporates both particle-fluid and particle-particle interaction via a Direct Forcing Method (DFM) and a hard sphere Discrete Particle (DP) approach. In our model a fixed (Eulerian) grid is utilized to solve the Navier-Stokes equations for the entire computational domain. The no-slip condition at the surface of the moving particles is enforced via a momentum source term which only acts in the vicinity of the particle surface. Specifically Lagrangian force points are used which are distributed evenly over the surface of the particle. Dissipative particle-particle and/or particle-wall collisions are accounted via a hard sphere DP approach using a three-parameter particle-particle interaction model accounting for normal and tangential restitution and tangential friction. The capabilities of the hybrid VOF-IB model are demonstrated with a number of examples in which complex topological changes in the interface are encountered.

### NOMENCLATURE

$d_p$	Particle diameter (-)
$d$	Plane constant for interface segment cutting through Eulerian cell (-)
$D$	Distribution or smoothing function (-)
$F$	Fractional amount of liquid (-)
$\tilde{F}$	Smoothed colour function (-)
$h$	Smoothing function stencil width (m) Measure for Eulerian grid size (m)
$I_p$	Moment of inertia (kg.m <sup>2</sup> )
$k$	Spring stiffness (N/m)
$m_p$	Particle mass (kg)
$N_p$	Number of force points per particle (-)
$n_i$	i <sup>th</sup> component of the unit normal vector (-)
$p$	Pressure (N/m <sup>2</sup> )
$t$	Time (s)
$x_i$	i <sup>th</sup> co-ordinate direction (m)
$x$	x co-ordinate (m)
$y$	y-co-ordinate (m)

$z$  z-co-ordinate (m)

### Greek letters

$\kappa$	Curvature (m <sup>-1</sup> )
$\mu$	Dynamic viscosity (kg/(m.s))
$\rho$	Density (kg/m <sup>3</sup> )
$\Delta\rho$	Density difference (kg/m <sup>3</sup> )
$\Delta x_i$	Grid spacing in i <sup>th</sup> co-ordinate direction (m)
$\Delta V$	Volume of computational cell (m <sup>3</sup> )
$\sigma$	Surface tension (N/m)
$\Delta t$	Time step (s)
$\Delta A_m$	Area of range of influence of force point m (m <sup>2</sup> )
$\Delta V_m$	Volume of range of influence of force point m (m <sup>3</sup> )

### Vectors

$\vec{f}_\sigma$	Volumetric surface tension force (N/m <sup>3</sup> )
$\vec{f}_{f \rightarrow s}$	Eulerian force density (N/m <sup>3</sup> )
$\vec{F}_{f \rightarrow s}$	Total force exerted by the fluid on the particle (N)
$\vec{F}_m$	Lagrangian force density (N/m <sup>3</sup> )
$\vec{g}$	Gravitational acceleration (m/s <sup>2</sup> )
$\vec{m}$	Normal vector
$\vec{n}$	Unit normal vector
$\vec{r}$	Position vector (m)
$\vec{T}_{f \rightarrow s}$	Torque exerted by fluid on the particle (N.m)
$\vec{u}$	Velocity (m/s)
$\vec{w}_p$	Particle translational velocity (m/s)
$\vec{W}_m$	Velocity at Lagrangian force point m (m/s)
$\vec{\omega}_p$	Particle rotational velocity (s <sup>-1</sup> )

### Subscripts and superscripts

1,2	Phase number
$m$	Marker
$x$	x-direction
$y$	y-direction
$z$	z-direction

### Operators

$\partial / \partial t$	Partial time derivative (s <sup>-1</sup> )
$D / Dt$	Substantial derivative (s <sup>-1</sup> )
$\nabla$	Gradient operator (m <sup>-1</sup> )
$\nabla \cdot$	Divergence operator (m <sup>-1</sup> )
$T$	Transpose of a tensor
$\otimes$	Cross vector product

## INTRODUCTION

Multi-fluid flows in which a sharp interface exists are frequently encountered in a variety of industrial processes. It has proven particularly difficult to accurately simulate these flows which can be attributed to i) the fact that the interface separating the fluids needs to be tracked accurately without introducing excessive computational smearing ii) the necessity to account for surface tension in case of (highly) curved interfaces iii) the incorporation of the no-slip boundary condition at the surface of (moving) solid bodies (particles). Roughly three differing approaches are possible which differ in the degree of sophistication. In the Eulerian approach the multi-fluid system is treated as interpenetrating continua with specified interactions between the phases whereas in the Lagrangian approach the dispersed elements (particles, drops or bubbles) are tracked individually taking into account the interactions with the continuous phase and other dispersed elements. This leads to the well-known and difficult closure problem in multiphase flows. In the DNS approach, of which the present VOF-IB method constitutes an example, all the relevant length and time scales are resolved and consequently these models can be helpful in testing and developing closure models which are required for the Eulerian and Lagrangian approach. This line of thought can in principle be used for any multiphase flow system and has been adopted by the authors for gas-solid (van der Hoef et al., 2004, 2006) and gas-liquid (Deen et al., 2004) dispersed two-phase flows.

The main emphasis in this paper is on the most fundamental level of modeling, namely the Direct Numerical Simulation (DNS) of multi-fluid flows, a field which has advanced considerably in the past decade due to the advances in numerical simulation techniques and computer hardware. The simulation model presented in this paper combines the salient features of the VOF model developed by van Sint Annaland et al. (2005) and the combined Immersed Boundary Discrete Particle (IB-DP) model. The Volume of Fluid (VOF) part features i) an interface reconstruction technique based on piecewise linear interface representation ii) a three-dimensional version of the CSF model of Brackbill et al. (1992). The Immersed Boundary (IB) part incorporates both particle-fluid and particle-particle interaction via a Direct Forcing Method (DFM) and a hard sphere Discrete Particle (DP) approach. Subsequently a brief review will be presented for the two main parts (i.e. the VOF model and the combined IB-DP model) of the present model.

*Volume of Fluid (VOF)* methods (Hirt and Nichols, 1981; Youngs, 1982; Rudman, 1997, 1998; Rider and Kothe, 1998; Scardovelli and Zaleski, 1999; Popinet and Zaleski, 1999; Bussman et al., 1999) employ a colour function  $F(x,y,z,t)$  that indicates the fractional amount of fluid present at a certain position  $(x,y,z)$  at time  $t$ . The evolution equation for  $F$  is usually solved using special advection schemes (such as geometrical advection, a pseudo Lagrangian technique), in order to minimize numerical diffusion. In addition to the value of the colour function the interface orientation needs to be determined, which follows from the gradient of the colour function. Roughly two important classes of VOF methods can be distinguished with respect to the representation of the interface, namely Simple Line Interface Calculation (SLIC) and Piecewise Linear Interface Calculation (PLIC). Earlier work is generally typified by the SLIC algorithm due to Noh and Woodward (1976) and the

Donor-Acceptor algorithm published by Hirt and Nichols (1981). Modern VOF techniques include the PLIC method due to Youngs (1982). The accuracy and capabilities of the modern PLIC VOF algorithms greatly exceeds that of the older VOF algorithms such as the Hirt and Nichols VOF method (Rudman, 1997). A drawback of VOF methods is the so-called artificial (or numerical) coalescence of gas bubbles which occurs when their mutual distances is less than the size of the computational cell. In this study we have adopted the Volume of Fluid (VOF) method based on a piecewise linear interface representation (PLIC VOF). Our model is based on Youngs' VOF method which gave the best overall performance in standard (two-dimensional) advection tests and simulations of (two-dimensional) Rayleigh-Taylor instability as reported by Rudman (1997). In our model relatively high values for the density and viscosity ratio (typically one hundred) can be used without an adverse effect on the stability and the required computational effort. Traditionally systems with a high density and viscosity ratio have proven difficult to simulate as reported by Scardovelli and Zaleski (1999) and Sabisch et al. (2001).

*Immersed Boundary (IB)* methods (Peskin, 1977; Saiki and Birlingen, 1996; Peskin, 2002; Mittal and Iaccarino, 2005) make use of a fixed Eulerian grid to solve for the flow field of the continuous phase and Lagrangian markers associated with the motion of the immersed body which can be of flexible or rigid nature. The IB method has been widely used to study fluid-structure interaction and was pioneered by Peskin (1977) to cardiac flow problems. In recent years the range of applications of this powerful computational method has expanded considerably. For excellent reviews the interested reader is referred to Peskin (2002) and Mittal and Iaccarino (2005). The advantages of the IB method are its flexibility with respect to incorporation of differing degree of rigidity (from elastic to rigid) of the bodies. Moreover, this method is relatively easy to implement. Disadvantages include the explicit treatment of the fluid-solid interaction which leads to stiffness problems for rigid particles. In addition appropriate values for the fluid-solid interaction parameters (such as the spring stiffness) need to be determined for each particular class of problems. The IB-DP part of our technique embeds a Direct Forcing Method (DFM), to enforce the fluid-solid coupling and a Discrete Particle (DP) method to account for the possible dissipative collisions between the suspended particles and confining walls.

Our fluid-solid coupling technique is similar in concept to the IB method developed by Feng and Michaelides (2005) and Uhlmann (2005). Contrary to Feng and Michaelides we use a finite difference technique to compute the flow field and contrary to Uhlmann we have incorporated a collision model to account for dissipative particle-particle and/or particle-wall collisions. The organisation of this paper is as follows: first the description of the model and the numerical solution method is given. Subsequently the verification of the method will be addressed. Then the results are presented and discussed and finally the conclusions are presented.

## GOVERNING EQUATIONS AND NUMERICAL SOLUTION METHOD

Our model consists of two main parts: one part deals with the presence of deformable interfaces (VOF model) whereas the other part accounts for the presence of the solid particles taking into account the possible non-ideal collisions between the particles themselves and/or confining walls (IB-DP model). First, the main conservation equations will be presented along with the incorporation of surface tension and the advection of the deformable interfaces. The fluid-solid coupling and the particle motion and (possible) collisional interaction will subsequently be described.

### Conservation equations

For incompressible multi-material flows the Navier-Stokes equations can be combined into a single equation for the fluid velocity  $\bar{u}$  in the entire domain (including the interior of the solid particles) of interest taking into account i) surface tension through a local volumetric surface tension force  $\bar{f}_\sigma$  (with dimension  $N/m^3$ ) accounting for the presence of curved deformable interfaces and ii) fluid-solid coupling through a momentum source term  $\bar{f}_{f \rightarrow s}$  (with dimension  $N/m^3$ ) accounting for the presence of the suspended solid particles and chosen in such a manner that the no-slip condition at the surface of the (moving) solid bodies (particles) is enforced. The governing conservation equations for unsteady, incompressible, Newtonian, multi-fluid flows are given by the following expressions:

$$(\nabla \cdot \bar{u}) = 0 \quad (1)$$

$$\rho \left[ \frac{\partial \bar{u}}{\partial t} + (\nabla \cdot \bar{u} \bar{u}) \right] = -\nabla p + \rho \bar{g} + (\nabla \cdot \mu [(\nabla \bar{u}) + (\nabla \bar{u})^T]) + \bar{f}_\sigma - \bar{f}_{f \rightarrow s}, \quad (2)$$

where the local averaged density  $\rho$  and viscosity  $\mu$  are evaluated from the local distribution of the phase indicator or colour function function  $F$  which is governed for by:

$$\frac{DF}{Dt} = \frac{\partial F}{\partial t} + (\bar{u} \cdot \nabla F) = 0 \quad (3)$$

expressing that the interface property is advected with the local fluid velocity. For the local average density  $\rho$  linear weighing of the densities of the continuous (2) and dispersed phase (1) is used:

$$\rho = F \rho_1 + (1 - F) \rho_2 \quad (4)$$

Similarly, the local average dynamic viscosity can also be obtained via linear averaging of the dynamic viscosities of the continuous (2) and dispersed phase (1). As an alternative, more fundamental approach recently proposed by Prosperetti (2001), the local average viscosity can be calculated via harmonic averaging of the kinematic viscosities of the involved phases according to the following expression:

$$\frac{\rho}{\mu} = F \frac{\rho_1}{\mu_1} + (1 - F) \frac{\rho_2}{\mu_2} \quad (5)$$

In all computations reported in this paper Eq. 5 was used to compute the local average viscosity. The volumetric surface tension force appearing in the momentum Eq. 2 acts only in the vicinity of the interface

### Surface tension

In the CSF model (Brackbill et al., 1992) the surface tension force acts via a source term  $\bar{f}_\sigma$  in the momentum equation which only acts in the vicinity of the interface. The expression for  $\bar{f}_\sigma$  is given by

$$\bar{f}_\sigma = 2F\sigma\kappa\bar{m} \quad (6)$$

where the expression for the curvature is obtained from the divergence of the unit normal vector to the interface:

$$\kappa = -(\nabla \cdot \bar{n}) = \frac{1}{|\bar{m}|} \left[ \frac{\bar{m}}{|\bar{m}|} \cdot \nabla |\bar{m}| - (\nabla \cdot \bar{m}) \right] \quad (7)$$

The normal to the interface is computed from the gradient of the smoothed colour function. The smoothing technique used in this paper will be discussed later.

### Advection of deformable interfaces

The integration of the hyperbolic F-advection equation is the most critical part of the VOF model and is based on geometrical advection which can be viewed as a pseudo-Lagrangian advection step. The advantage of the geometrical advection is given by the fact that a very sharp interface is maintained during the simulations. First for each Eulerian cell containing an interface the unit normal vector to the interface is estimated from the gradient of the colour function  $F$ :

$$\bar{n} = \frac{\nabla F}{|\nabla F|} \quad (8)$$

The number of possible interface configurations can be minimised from sixty four to five generic ones which are schematically shown in Fig. 1. From these five generic interface types the particular type prevailing in a certain Eulerian cell needs to be determined on basis of the known interface orientation (i.e. the normal vector to the interface) and the F-value of the interface cell. For the computation of the fluxes through the cell faces the equation for the planar interface segment cutting through the Eulerian cell needs to be considered. This equation is given by:

$$n_1 \xi_1 + n_2 \xi_2 + n_3 \xi_3 = d \quad (9)$$

where  $\xi_i$  ( $i = 1..3$ ) represents the dimensionless coordinate in direction  $i$  given by:

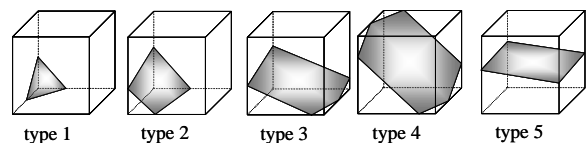


**Figure 1:** Five generic types of interface configurations considered in the computation of the fluxes through the cell faces.

$$\xi_i = \frac{x_i}{\Delta x_i} \quad (10)$$

where  $\Delta x_i$  represents the grid-spacing in co-ordinate direction  $x_i$  ( $i = 1..3$ ). The value of the plane constant  $d$  can be determined by equating the expression for the dimensionless liquid volume (volume below the planar interface segments shown in Fig. 1) to the known fractional amount of liquid or the F-value in the interface cell. The value of  $d$  can be obtained readily from the root of these non-linear equations using the Newton-Raphson method which needs however to be done with care in order to find the correct root of the cubic equations. As an alternative the Regula Falsi method can be used, which requires however an interval in which the root can be found. This interval can be obtained on basis of the known interface orientation (i.e. components of the normal to the interface) and the fractional amount of liquid in the interface cell (i.e. the F-value) using simple geometrical considerations. One should keep in mind here that the solution of the non-linear equation needs to be carried out only for the interface cells.

Once the aforementioned steps have been taken, finally the amount of liquid fluxed through each of the faces of the Eulerian cells during a time step  $\Delta t$  can be computed. The F-advection equation is discretised with an explicit treatment of the convections terms, where a straightforward generalisation of the 2D geometrical advection method given by Delnoij (1999) is used (also see Scardovelli and Zaleski, 1999). In our implementation of this method we have adopted the split advection scheme. Because the expressions for the fluxes through the cell faces are quite lengthy they are not given here. Finally the computed new F-values are corrected for (small) non-zero divergence of the velocity field due to the iterative solution of the Pressure Poisson Equation (PPE).

### Smoothing of the colour function $F$

As indicated before the interface orientation (i.e. the normal to the interface) is computed from the gradient of the color function  $F$  according to Eq. 8. Basically this involves numerical differentiation of a discontinuous function leading in practice to (small) inaccuracies. This problem can be overcome however by making use of a smoothed color function  $\tilde{F}$  for the computation of the unit normal to the interface using Eq. 8 with  $F$  replaced by  $\tilde{F}$  obtained from:

$$\tilde{F}(\bar{x}) = \sum_m D(x - x_m) D(y - y_m) D(z - z_m) F(\bar{x}_m) \quad (11)$$

where the smoothing function  $D$  is given by the function proposed by Peskin (1977):

$$D(x) = \frac{1}{2h} \left( 1 + \cos\left(\pi \frac{x}{h}\right) \right) \quad (12)$$

or as an alternative by a suitable polynomial expression as the one proposed by Deen et al. (2004):

$$D(x) = \frac{15}{16} \frac{1}{h} \left[ \left(\frac{x}{h}\right)^4 - 2\left(\frac{x}{h}\right)^2 + 1 \right] \quad (13)$$

where  $h$  represents the width of the computational stencil used for the smoothing. The summation in Eq. 11 only involves the grid points with distance (in each separate co-ordinate direction) equal or less than the smoothing or filter width  $h$ . We typically use  $h = 2\Delta$  where  $\Delta$  represents the Eulerian grid size and, unless otherwise stated. The width of the computational stencil for the smoothing should be selected carefully. When the width is too small numerical instabilities may arise, especially in case the coefficient of surface tension is high. On the other hand when the width of the computational stencil is chosen too large, excessive smoothing (“thickening” of the interface) is obtained which is undesirable. For the simulations reported in this paper we used Eq. 13 and additionally we used the smoothed colour function  $\tilde{F}$  instead of  $F$  in Eq. 6. It should be stressed here that this smoothed colour function is only used in conjunction with the estimation of the unit normal to the interface and not in the computation of the material fluxes through the faces of the computational cells for which the unsmoothed colour function was used.

### Fluid-solid coupling

The momentum source term  $\bar{f}_{f \rightarrow s}$  (with dimension  $N/m^3$ ) accounts for the presence of the suspended solid particles and is chosen such that the no-slip condition at the surface of the (moving) particles is accounted for. The computation of  $\bar{f}_{f \rightarrow s}$  constitutes an important element of the model and requires first the calculation of the Eulerian momentum density  $\rho^n \bar{u}^n$  from the available data at the old time level  $n$ .

$$\rho^n \bar{u}^n = \rho^n \bar{u}^n + \Delta t [\rho^n \bar{g} - \rho^n (\nabla \cdot \bar{u}^n \bar{u}^n) - \nabla p^n + \nabla \cdot \mu^n ((\nabla \bar{u}^n) + (\nabla \bar{u}^n)^T) + \bar{f}_\sigma^n] \quad (14)$$

The Eulerian momentum density is subsequently mapped to the Lagrangian force point  $m$  using a distribution function  $D$  to obtain the Lagrangian momentum density  $\rho^n \bar{U}_m^n$ :

$$\rho^n \bar{U}_m^n = \sum_k D(\bar{r}_k - \bar{r}_m) \rho^n \bar{u}^n(\bar{r}_k) \quad (15)$$

where  $\bar{r}_k$  and  $\bar{r}_m$  represent respectively the Eulerian velocity node  $k$  and the Lagrangian force point  $m$  residing on the surface of the particle. Unlike the traditional IB method, the Lagrangian force points reside at the surface of the particles and are moved with the particle velocities and not with the interpolated fluid velocity. The Lagrangian points are distributed in a uniform manner over the surface of the particles. For the distribution function  $D$  we use again volume-weighting. It should be added here that, due to the staggered grid used for the flow computation, the mapping given by Eq. 15 should be carried out separately for each component of the momentum density. Subsequently the velocity of the Lagrangian force point  $m$  is computed from the combined effect of particle translation and particle rotation:

$$\bar{W}_m = \bar{w}_p + (\bar{\omega}_p \otimes (\bar{r}_m - \bar{r}_p)) \quad (16)$$

where  $\bar{r}_m$  and  $\bar{r}_p$  respectively denote the position vector of Lagrangian force point m and the position vector of the center of particle p, whereas the translational and rotational velocities are respectively given by  $\bar{w}_p$  and  $\bar{\omega}$ .

The force density at the Lagrangian force point m is then obtained from:

$$\bar{F}_m = \frac{\rho^n \bar{W}_m - \rho^n \bar{U}_m}{\Delta t} \quad (17)$$

Finally the Eulerian force density is obtained by mapping the Lagrangian force density  $\bar{F}_m^*$ , related to  $\bar{F}_m$  by the following equations:

$$\bar{F}_m^* = \frac{\Delta V_m}{h^3} \bar{F}_m = \left[ \frac{\pi}{3N_p} \left[ 12 \left( \frac{R}{h} \right)^2 + 1 \right] \right] \bar{F}_m \quad (18)$$

for a sphere, to the Eulerian mesh. Again this mapping needs to be carried out for each component of the force density separately and needs to be summed over all  $N_p$  Lagrangian force points within a the range of influence of this point:

$$\bar{f}_{f \rightarrow s}(\bar{r}) = \sum_m D(\bar{r} - \bar{r}_m) \bar{F}_m^*(\bar{r}_m) \quad (19)$$

At this point we have at our disposal the spatial distribution of the Eulerian force density and we turn to the calculation of a tentative velocity field which accounts for the convective and diffusive momentum transport and all source terms excluding the pressure gradient:

$$\begin{aligned} \rho^n \bar{u}^{**} = & \rho^n \bar{u}^n + \Delta t [\rho^n \bar{g} - \rho^n (\nabla \cdot \bar{u}^n \bar{u}^n) + \\ & \nabla \cdot \mu^n ((\nabla \bar{u}^{**}) + (\nabla \bar{u}^{**})^T) + \bar{f}_\sigma^n - \bar{f}_{f \rightarrow s}] \end{aligned} \quad (20)$$

Eq. 20 is solved with a standard finite difference technique where the diffusion operator is approximated with standard central second order finite difference representations (mixed derivatives are evaluated explicitly) whereas the convection terms are computed with a second order flux delimited Barton-scheme (Centrella and Wilson (1984)). We use a robust and very efficient Incomplete Cholesky Conjugate Gradient (ICCG) algorithm to solve the resulting sparse matrix equation for each velocity component. The velocity field at the new time level n+1 is related to the tentative velocity field as follows:

$$\bar{u}^{n+1} = \bar{u}^{**} - \frac{\Delta t}{\rho^n} \nabla p^{n+1} \quad (21)$$

Since  $\bar{u}^{n+1}$  needs to satisfy the incompressibility constraint, upon taking the divergence of Eq. 21 the pressure Poisson equation is obtained:

$$(\nabla \cdot \frac{1}{\rho^n} \nabla p^{n+1}) = \frac{1}{\Delta t} (\nabla \cdot \bar{u}^{**}) \quad (22)$$

which again is solved with a robust and efficient ICCG algorithm to obtain the pressure at the new time level. From Eq. 21 finally the velocity field at the new time level is obtained which completes the computation of the fluid flow and the fluid-solid coupling.

### Particle motion and collisional interaction

The translational and rotational motion of the suspended solid particles is given by the Newtonian equations of motion respectively given by:

$$m_p \frac{d\bar{w}_p}{dt} = m_p \bar{g} + \bar{F}_{f \rightarrow s} \quad (23)$$

$$I_p \frac{d\bar{\omega}_p}{dt} = \bar{T}_{f \rightarrow s} a \quad (24)$$

where  $m_p$  and  $I_p$  represent respectively the mass and the moment of inertia of the particle. The final term on the right-hand side in Eq. 23 accounts for the drag force exerted by the fluid on the particle and is computed from:

$$\bar{F}_{f \rightarrow s} = \sum_{m=1}^{N_p} \bar{F}_m \Delta V_m \quad (25)$$

whereas the torque appearing at the right hand side of Eq. 24 is computed according to the following expression:

$$\bar{T}_{f \rightarrow s} = \sum_{m=1}^{N_p} (\bar{r}_m - \bar{r}_p) \times \bar{F}_m \Delta V_m \quad (26)$$

where  $\bar{F}_m$  and  $\Delta V_m$  respectively denote the force density at Lagrangian force point m given by Eq. 6 and the volume of the range of influence of this force point given by the following expression:

$$\Delta V_m = \frac{\pi h^3}{3N_p} \left[ 12 \left( \frac{R}{h} \right)^2 + 1 \right] \quad (27)$$

where h is the average Eulerian grid size and R the radius of the particle. The summation in Eqs. (25) and (26) is extended over all force points  $N_p$  distributed over the surface of the particle.

The source terms appearing in the Newtonian equations of motion are treated as known (explicit) terms and therefore the integration of these equations can be conducted in principle with any integration technique for ordinary differential equations. For the simulations reported in this paper we have used a second order trapezoidal rule producing translational and rotational velocities at the new time level computed respectively as follows:

$$\bar{w}_p^{n+1} = \bar{w}_p^n + \bar{g} \Delta t + \frac{\Delta t}{2m_p} [\bar{F}_{f \rightarrow s}^n + \bar{F}_{f \rightarrow s}^{n+1}] \quad (28)$$

$$\bar{\omega}_p^{n+1} = \bar{\omega}_p^n + \frac{\Delta t}{2I_p} [\bar{T}_{f \rightarrow s}^n + \bar{T}_{f \rightarrow s}^{n+1}] \quad (29)$$

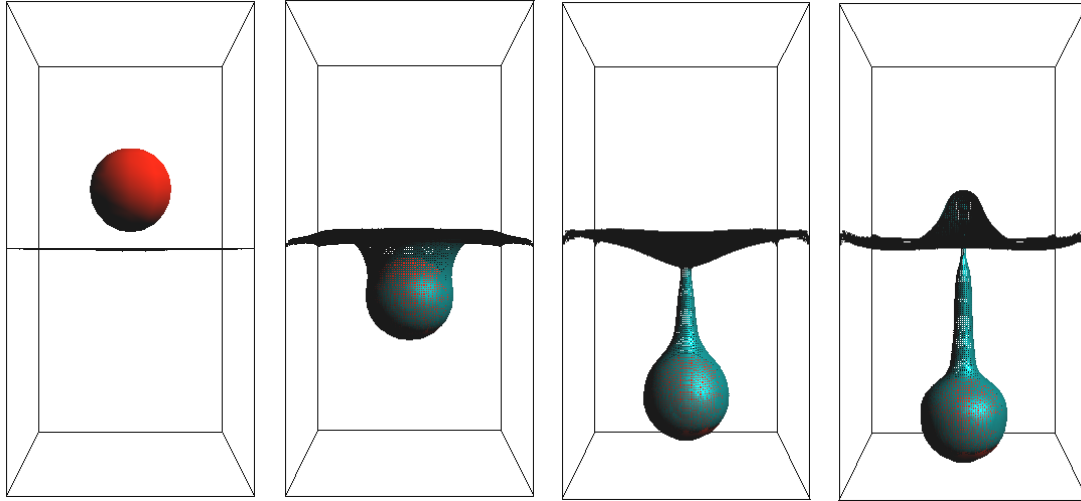


**Figure 2:** Snapshots at different times of the impact of a spherical particle (red) of 0.02 m diameter released on a flat surface of an initially quiescent liquid, using a 100x100x200 grid and a time step of  $5 \cdot 10^{-5}$  s. From left to right:  $t = 0.05$  s,  $t = 0.10$  s,  $t = 0.15$  s and  $t = 0.20$  s after release of the particle. Additional data are given in Table 3.

Once these new velocities are obtained an event driven hard sphere collision model is invoked. In this model it is assumed that the interaction forces are impulsive and therefore all other finite forces are negligible during collision. The closure of this collision model involves three micro-mechanical parameters: the coefficients for normal and tangential restitution and the tangential friction coefficient, which in principle can be obtained from impact experiments.

## VERIFICATION

The combined VOF-IB model was systematically tested to verify the correctness of the computer implementation. Van Sint Annaland et al. (2005) performed extensive calculations using their VOF-model for gas bubbles rising in quiescent viscous liquids and demonstrated that the computed terminal rise velocities and shapes of the bubbles agreed very well with those obtained from the Grace diagram over a very wide range of Eötvös and Morton numbers, while using a high density and viscosity ratio characteristic for gas-liquid systems. They also applied their model successfully to a case where the interface experiences substantial changes, i.e. co-axial and oblique coalescence of two gas bubbles rising in a viscous liquid and obtained good agreement with results published in literature. The IB-model was tested extensively by computing the terminal velocity of single spheres and the drag coefficient for static arrays of particles. In each case good agreement with data reported in literature was found.

## RESULTS

The technique presented in this paper can in principle be used for a broad range of complex multi-fluid flows such as gas-liquid two-phase flows through a (dense) packing of solid spheres encountered in for instance trickle flow reactors. In addition this technique can be used to study the microscopic phenomena relevant for fluid bed granulation. In this paper we report a number of test cases in which substantial changes in interface topology prevail, namely i) impact of a spherical particle on a flat liquid surface and ii) impact of a falling drop on a single spherical particle kept stationary iii) impact of a drop on a stationary array of spherical particles.

Computational grid	100x100x200 (-)
Grid size	0.0005 m
Time step	0.00005 s
Particle radius	0.01 m
Particle density	2000 kg/m <sup>3</sup>
Initial particle position	$(x_0, y_0, z_0) = (0.025, 0.025, 0.075)$ m
Liquid density	1000 kg/m <sup>3</sup>
Liquid viscosity	0.1 kg/(m.s)
Gas density	100 kg/m <sup>3</sup>
Gas viscosity	0.01 kg/(m.s)
Surface tension	0.1 N/m

**Table 1:** Parameters used for the impact simulation of a spherical particle on a flat liquid surface.

Computational grid	100x100x200 (-)
Grid size	0.0005 m
Time step	0.00005 s
Particle radius	0.005 m
Particle position	$(x_0, y_0, z_0) = (0.025, 0.025, 0.025)$ m
Drop radius	0.01 m
Drop position	$(x_0, y_0, z_0) = (0.025, 0.025, 0.075)$ m
Liquid density	1000 kg/m <sup>3</sup>
Liquid viscosity	0.1 kg/(m.s)
Gas density	100 kg/m <sup>3</sup>
Gas viscosity	0.01 kg/(m.s)
Surface tension	0.1 N/m

**Table 2:** Parameters used for the impact simulation of a drop on a stationary spherical particle.

Computational grid	80x80x160 (-)
Grid size	0.0005 m
Time step	0.00005 s
Particle radius	0.003 m
Particle array	cubic lattice of 5x5x5 particles (-)
Drop radius	0.01 m
Drop position	$(x_0, y_0, z_0) = (0.02, 0.02, 0.06)$ m
Liquid density	1000 kg/m <sup>3</sup>
Liquid viscosity	0.1 kg/(m.s)
Gas density	100 kg/m <sup>3</sup>
Gas viscosity	0.01 kg/(m.s)
Surface tension	0.1 N/m

**Table 3:** Parameters used for the impact simulation of a drop on a stationary array of particles.

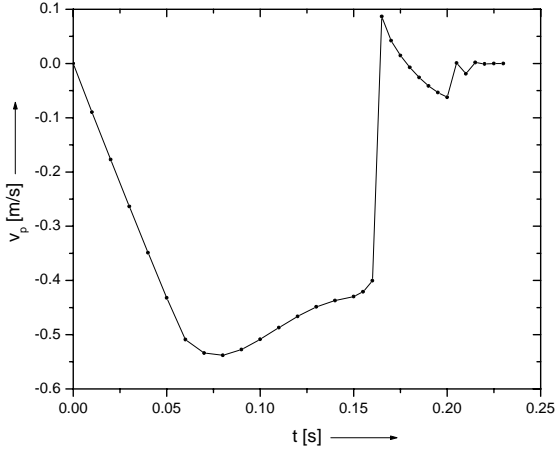


**Figure 3:** Velocity of the particle as a function of time showing acceleration in the gas phase (0-0.06 s) deceleration in the liquid phase (0.06-0.16 s) and inelastic collision with the bottom wall ( $t = 0.17$  s) followed by secondary collisions.

#### Impact of a spherical particle on a flat liquid surface

The impact of spherical particles on liquid surfaces has been studied experimentally by various researchers and constitutes a challenging test case for our hybrid VOF-IB method. For this simulation a system was considered in which the initially quiescent liquid phase occupies the bottom half of the computational domain. Initially the particle is at its rest position in the center of the gas cap present above the liquid surface and is released at  $t = 0$  s. For the simulation no-slip boundary conditions were imposed at the confining domain walls whereas the no-slip condition at the surface of the particle was imposed with the IB method. The data used for the simulation are detailed in Table 1.

In Fig. 2 a series of snapshots of the impact simulation are shown whereas in Fig. 3 the vertical velocity of the particle is given as a function of time. In Fig. 2 the interface is visualized with a surface mesh defined by the corner points of the polygons representing the interface segments at the level of the computational cells (see Fig. 1). Initially the particle accelerates in the gas phase and at  $t = 0.060$  s the bottom side of the particle impacts on the liquid surface causing its deformation. In the second frame ( $t = 0.100$  s) given in Fig. 2 the particle has moved completely below the surface of the liquid and a big open cavity has been formed behind the particle. Subsequently the particle descends through the viscous liquid while the cavity behind the particle closes rather slowly leading to the formation of a gas neck which is pinched off between  $t = 0.150$  and  $t = 0.155$  s. This phenomenon initiates the formation of an inverse (i.e. upward) motion of the liquid in the center leading to the formation of a mild jet. At the top of the remaining gas neck small bubbles are released which subsequently rise through the jet region. As long as the particle moves in the gas phase (see Fig. 3) it accelerates (terminal velocity in gas phase equals  $\sim 3$  m/s), however as soon as the particle contacts the liquid surface it decelerates due to the tenfold increase in density and viscosity in the liquid phase (terminal velocity in liquid phase equals  $\sim 0.5$  m/s). The particle finally hits the bottom wall of the container and comes to rest after a few inelastic collisions with the bottom wall.

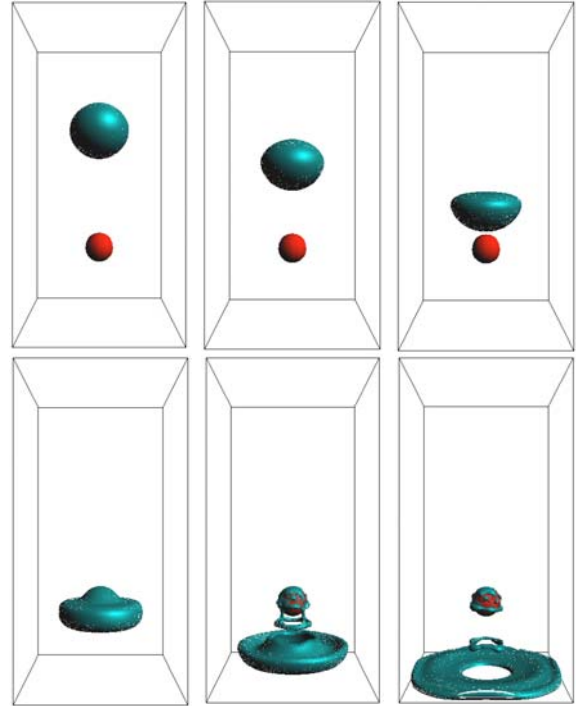


**Figure 4:** Snapshots at different times of the impact of a drop of 0.020 m diameter released on a spherical particle of 0.01 m kept at its original position. Computational grid:  $100 \times 100 \times 200$ ; time step:  $5 \cdot 10^{-5}$  s. Additional data are given in Table 4. Top (from left to right):  $t = 0.050$  s,  $t = 0.075$  s and  $t = 0.100$  s; Bottom (from left to right):  $t = 0.125$  s,  $t = 0.150$  s and  $t = 0.175$  s.

#### Impact of a drop on a single spherical particle

In the second example we simulate the impact of a large drop on a single stationary spherical particle. The drop was released from its initial position in the top part of the domain whereas the particle was kept at its stationary position in the bottom part of the domain (gas phase initially quiescent). For the simulation again no-slip boundary conditions were imposed at the domain walls, additional data used for the simulation are detailed in Table 2. In Fig. 4 a series of snapshots of the droplet impact on the stationary particle are shown. Upon impact of the drop a considerable shape deformation occurs where the drop attains a disk type shape with a central hole. During passage of this disk drop fragmentation commences where the main body of liquid moves around the particle whereas a residual amount of liquid initially adheres to the particle. Subsequently ring shaped liquid filaments are shed from the residual liquid which eventually start (see snapshot at  $t = 0.175$  s in Fig. 4) to break up into small liquid drops.

#### Impact of a drop on a stationary array of spherical particles

In the last example we simulate the impact of a large drop on a stationary array of spherical particles arranged in a simple cubic packing configuration. The drop was released from its initial position in the top part of the domain whereas the particle array was kept at its stationary position in the bottom part of the domain (gas phase initially quiescent). For the simulation again no-slip boundary conditions were imposed at the domain walls, additional data used for the simulation are detailed in Table 3. In Fig. 5 a series of snapshots of the droplet

impact on the array of particles are shown. As evident from this figure the big drop upon impact on the array of particles considerably stretches in the lateral direction followed by percolation of the liquid through the voids in the packing.

## CONCLUSIONS AND OUTLOOK

In this paper a simulation model has been presented for the Direct Numerical Simulation (DNS) of complex multi-fluid flows in which simultaneously (moving) deformable (drops or bubbles) and non-deformable (moving) elements (particles) are present, possibly with the additional presence of free surfaces. Our model combines the VOF model developed by van Sint Annaland et al. (2005) and the Immersed Boundary (IB) model and has been applied to the simulation of a number of cases in which substantial changes of the interface topology prevail. Our simulations qualitatively reproduce the observed phenomena but clearly extension and refinement of the model is required to incorporate for instance an accurate representation of the wetting properties of three-phase systems. In addition detailed experimental validation using well-defined experiments is still required. Once these steps have been taken, the model can be used to study for example liquid spreading in (structured) packings in a very detailed way. In this connection it should be stressed that the IB method offers considerable flexibility in representing geometrically complex structures.

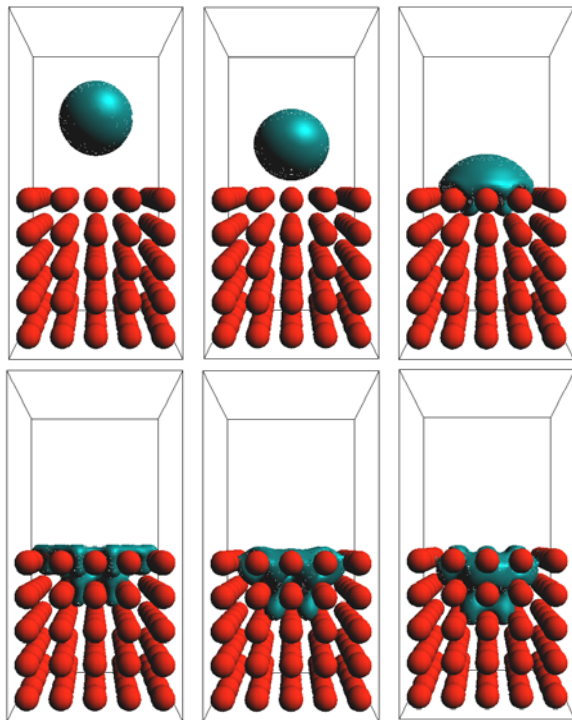


**Figure 5:** Snapshots at different times of the impact of a drop of 0.02 m diameter released on a stationary array of spherical particles kept at its original position. Computational grid: 80x80x160; time step:  $5 \cdot 10^{-5}$  s. Additional data are given in Table 5. Top (from left to right):  $t = 0.025$  s,  $t = 0.050$  s and  $t = 0.075$  s; Bottom (from left to right):  $t = 0.100$  s,  $t = 0.125$  s and  $t = 0.150$  s.

## REFERENCES

- BRACKBILL, J.U., KOTHE, D.B. and ZEMACH, C. (1992). A continuum method for modeling surface tension. *J. Comp. Phys.* **100**, 335.
- BUSSMAN, M., MOSTAGHIMI, J. and CHANDRA, S. (1999). On a three-dimensional volume tracking model of droplet impact. *Phys. Fluids*, **11**, 1406-1417.
- CENTRELLA, J. and WILSON, J. (1984). Planar numerical cosmology. II. The difference equations and numerical tests, *Astrophysical J. Suppl. Ser.* **54**, 229.
- DEEN, N.G., VAN SINT ANNALAND, M. and KUIPERS, J.A.M. (2004). Multi-level modelling of dispersed gas-liquid two-phase flow, *Chem. Eng. Sci.* **59**, 1853-1861.
- DELNOIJ, E. (1999). Fluid dynamics of gas-liquid bubble columns: a theoretical and experimental study, PhD thesis, Twente University, The Netherlands.
- FENG, Z.G. and MICHAELIDES, E. (2005). Proteus: a direct forcing method in the simulations of particulate flows, *J. Comp. Phys.*, **202**, 20-51.
- HIRT, C.W. and NICHOLS, B.D. (1981). Volume of Fluid (VOF) method for the dynamics of free boundaries, *J. Comp. Phys.* **39**, 201.
- HOOMANS, B.P.B., KUIPERS, J.A.M., BRIELS, W.J. and van SWAAIJ, W.P.M. (1996). Discrete particle simulation of bubble and slug formation in a two-dimensional gas-fluidised bed: A hard sphere approach, *Chem. Eng. Sci.* **51**, 99-108.
- MITTAL, R. and IACCARINO, G. (2005). Immersed boundary methods, *Annu. Rev. Fluid Mech.*, **37**, 239-261.
- NOH, W.F. and WOODWARD, P.R. (1976). SLIC (Simple Line Interface Calculation) method, In: *Lecture Notes in Physics*, A.I. van de Vooren and P.J. Zandbergen (eds.), 330.
- PESKIN, C.S. (1977). Numerical analysis of blood flow in the heart, *J. Comp. Phys.*, **25**, 220-252.
- PESKIN, C.S. (2002). The immersed boundary method, *Acta Numerica*, 479-517.
- POPINET, S. and ZALESKI, S. (1999). A front-tracking algorithm for accurate representation of surface tension. *Int J. Numer. Meth. Fluids*, **30**, 775-793.
- PROSPERETTI, A. (2001). Navier-Stokes numerical algorithms for free-surface flow computations: An overview. *Drop Surface Interactions*, 21.
- RIDER, W.J. and KOTHE, D.B. (1995). Stretching and tearing interface tracking methods, Los Alamos National Laboratory, Available on World Wide Web at: [http://laws.lanl.gov/XHM/personnel/wjr/Web\\_papers/pubs.html](http://laws.lanl.gov/XHM/personnel/wjr/Web_papers/pubs.html).
- RIDER, W.J. and KOTHE, D.B. (1998). Reconstructing volume tracking, *J. Comp. Phys.*, **141**, 112-152.
- RUDMAN, M. (1997). Volume-tracking methods for interfacial flow calculations, *Int. J. Num. Methods in Fluids*, **24**, 671-691.
- RUDMAN, M. (1998). A volume-tracking method for incompressible multifluid flows with large density variations. *Int. J. Num. Methods in Fluids*, **28**, 357-378.
- SABISCH, W., WÖRNER, M., GROTZBACH, G. and CACUCCI, D.G. (2001). Driedimensionale numerische Simulation von aufsteigenden Einzelblasen und Blasenschwämen mit einer Volume-of Fluid-Methode, *Chemie Ing. Techn.*, **73**, 368-373.
- SAIKI, E.M. and BIRLINGEN, S. (1996). Numerical simulation of a cylinder in uniform flow: application of a virtual boundary method, *J. Comp. Phys.*, **123**, 450-465.

SCARDOVELLI, S. and ZALESKI, S. (1999). Direct numerical simulation of free-surface and interfacial flow, *Annu. Rev. Fluid Dyn.*, **31**, 567-603.

UHLMANN, M. (2005). An immersed boundary method with direct forcing for the simulation of particulate flows, *J. Comp. Phys.*, **209**, 448-476.

VAN DER HOEF, M.A., VAN SINT ANNALAND, M. and KUIPERS, J.A.M. (2004). Computational fluid dynamics for dense gas-solid fluidized beds: a multi-scale modeling strategy, *Chem. Eng. Sci.*, **59**, 5157-5165.

VAN DER HOEF, M.A., YE, M., VAN SINT ANNALAND, M., ANDREWS, A.T., SUNDARESAN, S. and KUIPERS, J.A.M. (2006). Multi-scale modeling of gas-fluidized beds, *Adv. Chem. Eng.*, **31**, 65.

VAN SINT ANNALAND, M., DEEN, N.G. AND KUIPERS, J.A.M. (2005). Numerical Simulation of Gas Bubbles Behaviour Using a Three-Dimensional Volume of Fluid Method, *Chem. Eng. Sci.*, **60**, 2999-3011.

YOUNGS, D.L. (1982). Time-dependent multi-material flow with large fluid distortion, In: *Numerical methods for fluid dynamics*, K.W. Morton and M.J. Baines (Eds.), Academic Press, New York, 273-285.